The International Journal of Advanced Manufacturing Technology (2023) 128:2301–2310
https://doi.org/10.1007/s00170-023-11876-2

ORIGINAL ARTICLE

Detailed characterisation of batch-manufactured flexible micro-grinding tools for electrochemical assisted grinding of copper surfaces

Lukas Steinhoff[1] · Rico Ottermann[1] · Folke Dencker[1] · Marc Christopher Wurz[1]

Received: 3 April 2023 / Accepted: 30 June 2023 / Published online: 5 August 2023

Abstract
Precision machining is becoming more and more important with the increasing demands on surface quality for various components. This applies, for example, to mirror components in micro-optics or cooling components in microelectronics. Copper is a frequently used material for this purpose, but its mechanical properties make it difficult to machine. In this study, a process strategy for finishing copper surfaces with batch-manufactured micro-grinding tools in an electrochemically assisted grinding process is demonstrated. The tool heads are manufactured from a polyimide-abrasive-suspension and silicon as a carrier substrate using microsystems technology. The matching shafts are milled from aluminium. The tools are then used on pure copper and oxidised copper surfaces. By using finer abrasives grains (1.6–2.4 µm instead of 4–6 µm) than previously, similar surface roughness values could be achieved ($R_a = 0.09 \pm 0.02$ µm, $R_z = 1.94 \pm 0.73$ µm) with the same grinding process. An optimised grinding process that combines the use of rough and fine tools, on the other hand, achieves significantly better surface finishes in just four grinding iterations ($R_a = 0.02 \pm 0.01$ µm, $R_z = 0.83 \pm 0.21$ µm). In order to achieve a further increase in surface quality, this optimised grinding process is combined with the anodic oxidation of the copper workpieces. The surface modification is done to increase the machinability of the surface by creating an oxide layer. This is confirmed by the results of scratch tests carried out, which showed less force acting on the tool during machining with the oxide layer than with a pure copper surface. To realise this within the machine tool, an electrochemical cell is shown that can be integrated into the machine so that the oxidation can be carried out immediately before the grinding process. The copper layers produced inside the electrochemical cell in the machine tool show similar characteristics to the samples produced outside. Processing the oxidised samples with the optimised grinding process led to a further reduction of about 17% in the R_z values ($R_a = 0.03 \pm 0.01$ µm, $R_z = 0.69 \pm 0.20$ µm). The combination of the shown grinding process and the integration of anodic oxidation within the machine tool for the surface modification of copper workpieces seems to be promising to achieve high surface finishes.

Keywords Micro-grinding · Precision engineering · High-precision machining · Micro production technology

1 Introduction

Technological progress is also accompanied by higher demands on manufacturing technology. This applies not only to macroscopic systems, but also to microsystems. In precision machining, this concerns mechanical processing in the fields of optics, biomedical technology and electronics, among others. For example, the proportion of scattered light in optical lenses must be kept as low as possible, or else the loss factor is too high. This can be achieved by reducing unwanted surface roughness [1]. Finishing the surface after milling can therefore be advantageous in order to increase the surface quality and the functionality of the component. A

✉ Lukas Steinhoff
steinhoff@impt.uni-hannover.de

Rico Ottermann
ottermann@impt.uni-hannover.de

Folke Dencker
dencker@impt.uni-hannover.de

Marc Christopher Wurz
wurz@impt.uni-hannover.de

[1] Institute for Micro Production Technology, An Der Universitaet 2, 30823 Garbsen, Germany

simple approach here is to connect a grinding process to the milling process in order to be able to reduce the roughness locally, where the functional area of the component is. In the field of micromachining, grinding is counted among the mechanical methods [2]. However, the machining of some materials can be difficult. This is a particular disadvantage with copper [3]. Due to its convincing properties, such as its high reflectivity for mirrors in optics or its high electrical and thermal conductivity for components in microelectronics such as high-power circuits, supply lines or cooling structures, it is a regularly used material in microsystems. In order to achieve a better machining result on copper surfaces, the right grinding tool is required on the one hand. A suitable surface modification on the other hand can also improve the machinability, as copper oxides are less ductile.

Grinding tools with flexible bond matrices offer the advantage that they are well suited for finishing. Due to the flexibility, the tool conforms to the surface contour and thus reduces the amount of material removed while retaining the structural geometry of the machined surface [4]. Micro-grinding tools with a flexible bonding matrix of polyimide and inserted silicon carbide (SiC) as abrasive particles have already been successfully batch-produced and used on copper. The machined copper surfaces showed a high improvement of the surface quality after only one grinding step, which could be further improved by more following steps [5]. However, the surface roughness values seemed to run into a limit after a while by using the micro-grinding tools with a grain size of 4–6 µm, which is why tools using a finer abrasive grit are presented in this study. Other micro-grinding tools often use diamond as an abrasive and can be produced by various methods, such as chemical vapour deposition [6] or electroless plating [7]. However, these are usually manufactured one by one, which means that the cost per grinding tool is higher. Similarly, diamond is not suitable for machining steel, because at higher temperatures, the carbon diffuses into the steel and the diamond is destroyed.

A modification of the copper surface can lead to a change in the mechanical properties, which can decrease the ductility of the pure copper and increase the machinability. Anodically oxidised copper, which contains various copper oxide compounds, shows a nanoneedle structure on the modified surface under certain manufacturing parameters. These nanoneedles show a more brittle behaviour and are mechanically less stable compared to the pure copper [8]. This leads to better machinability and therefore enables a higher surface quality to be achieved. Furthermore, the process of anodic oxidation offers the advantage that the roughness peaks in particular react more strongly on the copper surface to be oxidised, as a higher current density is applied to the roughness peaks due to the geometry [9]. As the roughness peaks are more oxidised than the solid material, they can be better removed, resulting in a stronger levelling of the surface through the grinding process, as could already be shown on the basis of the measured R_z values [10]. In addition, SiC as an abrasive showed better performance on the oxidised copper than cubic boron nitride. In order to be able to guarantee high-precision machining, it is necessary that the workpiece does not have to be repositioned after milling and before grinding for oxidation, as this can result in new tolerances, which leads to higher deviations in the structure geometry. Therefore, in this study, an experimental setup is shown how anodic oxidation can be carried out directly in the machine tool with a subsequent grinding process with batch-manufactured flexible micro-grinding tools.

2 Experimental procedure

The following section is divided into three subsections. First, the production of the micro-grinding tools is described, and then the anodic oxidation of copper surfaces and the design and construction of the electrochemical chamber for the machine tool is explained. Finally, the grinding tests and the associated analyses are specified.

2.1 Manufacturing of micro-grinding tools

The manufacturing process of the tools is divided into three parts, as shown in Fig. 1. In the first step, the suspension for the abrasive layer is mixed in order to be able to produce the tool heads. The polyimide-abrasive-suspension (PAS) is composed of 75 wt% polyimide (LTC9320, Fujifilm) and 25 wt% abrasive particles. Therefore, silicon carbide (SiC) is used in different grain sizes. In this work, the sizes 4–6 µm and 1.6–2.4 µm are used. The particles have a heterogeneous size and cutting-edge distribution. A homogeneous distribution of the abrasive within the polyimide is achieved by a gentle 10 min manual stirring process. In the second process step, the PAS is then spun onto a silicon wafer (500 rpm, 5 s; 1000 rpm, 25 s), whereby a uniform distribution of the viscous suspension is achieved. After a resting phase (10 min) and the softbake (70 °C, 10 min; 100 °C, 10 min), the structuring of the photostructurable polyimide follows by means of UV exposure (450 s). The basic structure of the micromills describes a circle, with a diameter of 1 mm. After a further resting phase (20 min), the PAS is developed using bath development with cyclopentanone and propylene glycol methyl ether acetate. After the grinding layer has been structured, an etching step is carried out to increase the subsequent cutting depth. For this purpose, a column with a total depth of approximately 250 µm including the thickness of the grinding layer is etched by means of deep reactive ion etching (DRIE). The grinding layer itself serves as an etching mask. Subsequently, the individual structures with a footprint of 1.2×1.2 mm^2 are separated by dicing.

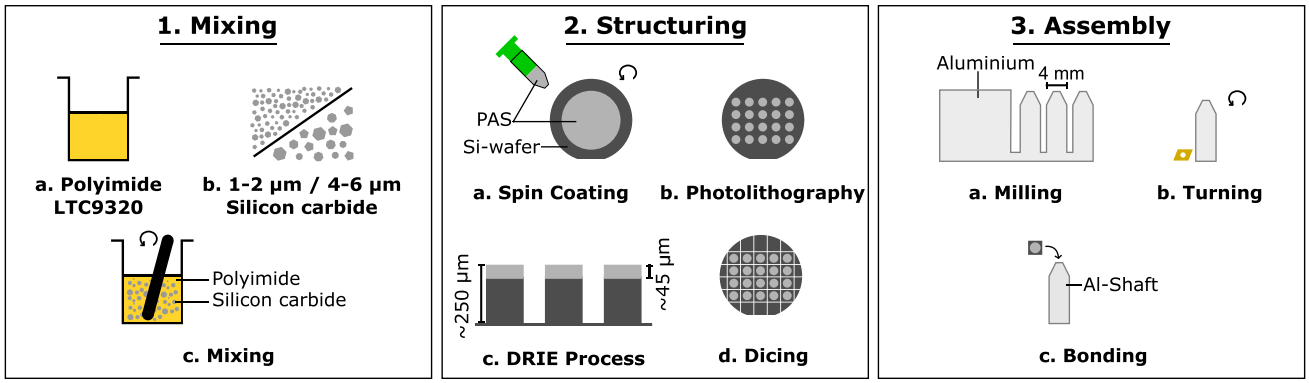

Fig. 1 The diagram describes the three-part manufacturing process of the micro-grinding tools. First, the PAS is prepared, and then the tool heads are structured. After that, the tool head and shaft are bonded together

Scanning electron microscopy (SEM) is used to compare the topography of the finished micro-grinding tool heads to get an impression of the conditioned surface and the size of the abrasive grains. Furthermore, the abrasive grain distribution of the 4–6 µm grains in the binding matrix is analysed by means of computer tomography (Xradia 520 Versa, Zeiss, Institut für Werkstoffkunde (Materials Science)) within the PAS. For this purpose, the tool head is exposed to X-rays, and the SiC and bond matrix can be distinguished on the basis of the contrast. The higher the material density, the brighter the greyscales in the captured image. By means of false colours and subsequent voxel counting, the proportions of abrasive to polymer can be calculated.

In the last part of the manufacturing process, the tool shafts are milled from a block of aluminium. The aim is to achieve an outer diameter of 4 mm so that the tools can later be used in standard tool holders. On the tip, the later joining place, a pocket is inserted to help align and centre the tool heads. A following turning step of the cylinder wall increases the concentricity of the shafts. Finally, the tool head is bonded to the tool shaft using 2 K epoxy resin adhesive (Plus Endfest 300, UHU).

An overview of the influence of different manufacturing parameters on the mechanical properties and the suitability of the adhesive has already been described [5].

2.2 Anodic oxidation of copper surfaces

The workpieces on which the following grinding tests are carried out are machined to a size of $25 \times 25 \times 6$ mm^3. The surface is then ground with FEPA P 1200 sandpaper to achieve a reference surface roughness, which is used to evaluate the success of the grinding process.

The electrochemical modification of the copper surface takes place after the sample preparation by using anodic oxidation. This is intended to improve the machinability of the surface of the copper workpiece due to the formation of an oxide layer. A three-electrode configuration is used for this purpose. The copper workpiece is connected as the working electrode (WE). A platinised titanium grid is used as the counter electrode (CE), which is attached parallel to the copper surface. The reference electrode (RE) is represented by an Ag/AgCl electrode, which is brought as close as possible to the WE. The reaction takes place in an alkaline environment consisting of NaOH with a concentration of 2 mol/L. Using a potentiostat, a potential of − 200 mV is then applied between RE and WE, which is held for 10 min. To keep the current density at the potential as high as possible, all conductive surfaces where no reaction is to take place are insulated. Thus, an oxide layer thickness of 5 µm is produced on average. This process is carried out in a laboratory fume hood in a beaker. Distilled water is used for the cleaning of the copper surface and nitrogen for drying. After production, the sample can be subjected to annealing by means of temperature treatment in order to transform the copper oxide layer. In the following analysis procedures, it should then be shown whether the annealed oxide layer would be more suitable for machining than the one that has not undergone any temperature treatment. For this purpose, the layer was treated for 3 h at 200 °C. The surface is examined by SEM, and the chemical composition of the oxide layer is analysed by X-ray photoelectron spectroscopy (XPS). Furthermore, it was investigated whether a cutting tool needs less force to drive through an oxide layer than through pure copper. This is to be interpreted as an index for the machinability of the layers. For this purpose, five pure copper, five oxidised copper, and five annealed copper oxide samples were machined with an indexable insert in a tribometer (UMT, Bruker). The tool was pressed into the material with a low force F_z of 0.2 N in order to machine only the top layer. The force F_x needed to drive the tool through the workpiece was recorded. The five recorded curves per sample type are then averaged and compared with each other.

A schematic design for performing anodic oxidation within the machine tool for more precise machining and uninterrupted process control is shown in Fig. 2A. The set-up is similar to the one already described, which is carried out outside the machine tool. A three-electrode design is used. The CE and the RE are attached in the lid of the electrochemical chamber. The WE is set onto a contacting plate by use of a clamping device and can thus be electrically contacted outside the chamber. The chamber has one fluid inlet and two outlets. The height of the outlets can be used to control whether the chamber is to be flooded or emptied. The chamber can be clamped in the machine tool (C5, Datron) by using a clamping and indexing pin. It has an overall dimension of 72 × 90 × 75 mm. Since the process is carried out with sodium hydroxide, the materials used must be resistant to it. Polypropylene is therefore used for the plastic components and stainless steel for the conductive metal components. To keep the reaction area as small as possible, all conductive surfaces that are not needed for the reaction are covered with an insulating, chemical-resistant adhesive tape. For the following grinding process, the chamber is rinsed with distilled water, and the lid together with CE and RE are removed so that the grinding tool can reach the modified copper surface. Before further oxidation, the chamber is then cleaned again with distilled water to remove possible contamination from grinding. The installed chamber with the connected electrodes and the attached lid is also shown in Fig. 2B.

2.3 Grinding tests

For the grinding tests, the workpieces are machined with the micro-grinding tools in the machine tool. First, a grinding test with finer-grained tools is carried out analogous to the previously published grinding tests [5]. To do this, the same tool is first used to grind a circle with a radius of 4 mm either once, four times or seven times, which corresponds to a tool path per iteration of 42.14 mm. An infeed of 5 µm, a cutting speed of 62 m/min, and a feed rate of 100 mm/min are used. After each iteration, a tool length measurement is performed using the machine tool to compensate for any tool wear and to maintain the 5 µm infeed. Furthermore, the grinding strategy is optimised by first performing two grinding steps with coarse-grained grinding tools (4– 6 µm grain size) and then two further grinding steps with finer-grained tools (1–2 µm grain size). This is carried out on a normal copper surface and on a copper surface oxidised in the machine tool. The ground surfaces are then analysed for their surface roughness using confocal microscopy (VK-9700, Keyence). The measurements are taken with a 50 × objective lens with a numerical apartur of 0.95. The mean roughness R_a and the mean roughness depth R_z are evaluated by the software (Analyse software, Keyence) according to ISO 4287:1997

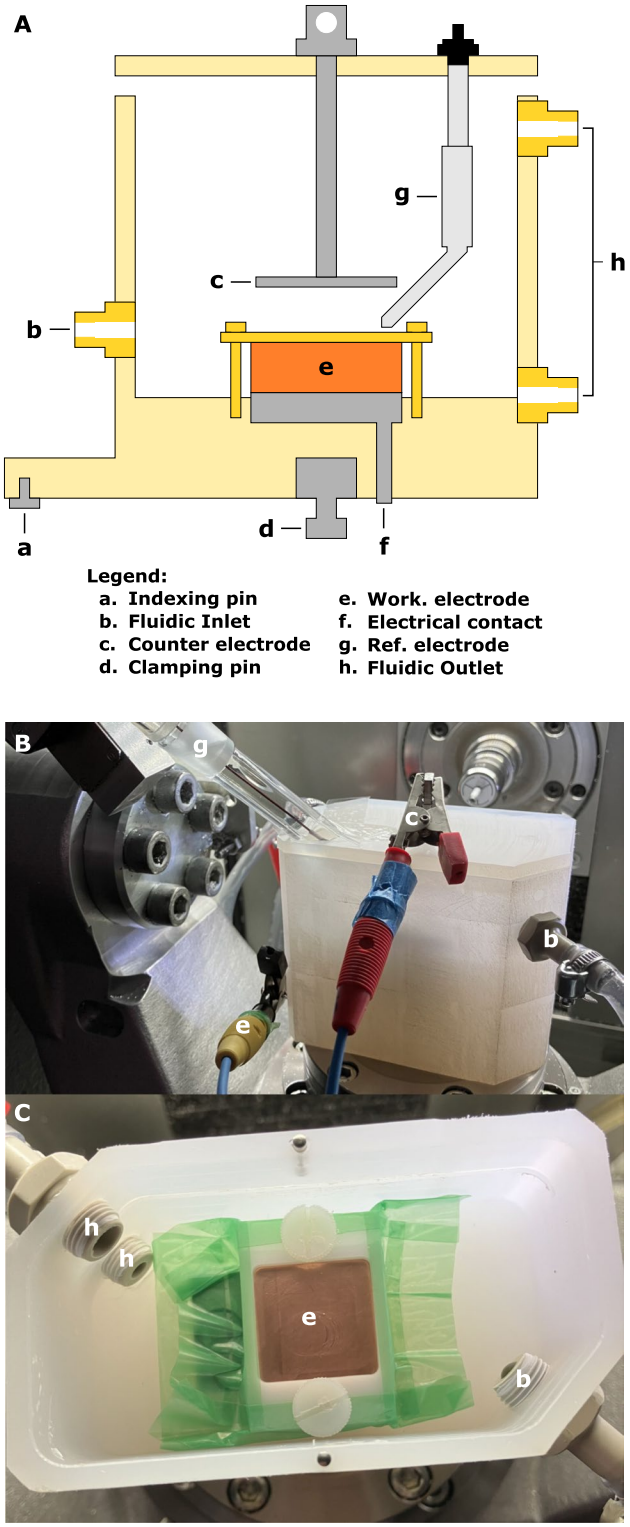

Fig. 2 **A** shows a schematic cross-section of the electrochemical chamber for the anodic oxidation of copper within the machine tool. The individual elements are labelled via the legend. In **B**, the installed chamber in the machine tool is shown, and **C** provides a view into the ready-to-use inside of the chamber

[11]. Three tests were run for each measuring point, and two roughness measurements were taken for each measured surface. The mean value is then calculated from the resulting six measurements.

3 Results and discussion

In the following, the results of the production of the micro-grinding tools, then the production of the oxidised copper workpieces and finally the analysis of the grinding tests are described and discussed.

3.1 Characterisation of the micro-grinding tools

The topography of a tool can influence the grinding result. Using SEM images from Fig. 3, the topographies of the grinding tools with two different grain sizes can be compared. Figure 3A shows a grinding tool with 4–6 µm grains. It is noticeable that the grains partially exceed 6 µm in one direction. This can lead to larger cutting edges and thus higher material removal during grinding, as was also shown in [10]. Topographically, however, the grains in this ready-to-use grinding head are evenly distributed and hardly covered with binding matrix on the surface due to the DRIE process. Thus, the cutting edges stand widely out of the matrix and can thus grind deeply into the workpiece, but also break out more quickly, so that this effect can only be observed at the beginning of a grinding process. Subsequent self-conditioning releases new abrasive grains, which are, however, more strongly bound into the polymer. In Fig. 3B, on the other hand, the topography of a micro-grinding tool is shown, which was produced with 1.6–2.4 µm grains. The distribution of the grain size seems to be much more homogeneous and within the desired range. However, grains that are significantly larger than 2.4 µm in one direction can also be detected here. Due to the DRIE step, the grains are hardly covered by binding matrix as well. This should result in the same effect as mentioned before. A uniform grain distribution can also be observed. Furthermore, due to the smaller grain size and thus the smaller cutting edges, a lower material removal per grinding iteration can be expected for the tools, but also finer scratches on the surface of the material. This should lead to reduced surface roughness.

In addition to the topography of the grinding tool, the abrasive grain distribution can also lead to a worse grinding result. During the production of the micro-grinding tools, the abrasive grains are stirred into the polymer by hand. There is a risk that the particles agglomerate. Therefore, an analysis of the grain distribution of the 4–6 µm grains is carried out by means of computer tomography. The captured images are coloured using false colours to be able to determine the percentages of each fraction. An SEM picture of an exemplary surface of a micro-grinding head and of two evaluated images of cross-sections is shown in Fig. 4.

Based on the two images, a homogeneous grain distribution without large agglomerate formation can already be recognised. The grains are evenly distributed throughout the abrasive layer. This is a good prerequisite for uniform cutting behaviour during machining and also for uniform tool wear. This makes the use of the manufactured tools more predictable and reduces the risk of a surface defect within the machined workpiece due to misbehaviour caused by agglomerated abrasive grains. Furthermore, the proportion of SiC in the bonding matrix can also be determined by this analysis. During the manufacturing process, there is a volume loss of the polymer due to solvent vaporisation and polymerisation, whereas the volume of SiC remains the same. By comparing the number of voxels in each slice for SiC and the bonding matrix, a percentage ratio between the two can then be calculated. For example, in Fig. 4A, the proportion of SiC is 51.9%, and in B, it is 55.9%. Over the entire grinding layer, the ratio is 54.3% SiC and 45.7% bond matrix. When mixing the PAS with 25 m% SiC, the ratio was 11.1% SiC and 88.9% bonding matrix. This strong change in the ratio can be explained mainly by the processing of the polymer. Due to the evaporation of the solvent portion during softbake and hardbake, a high volume of the binding matrix is lost. This results in more cutting edges being present in the cutting plane, and thus, a higher metal removal

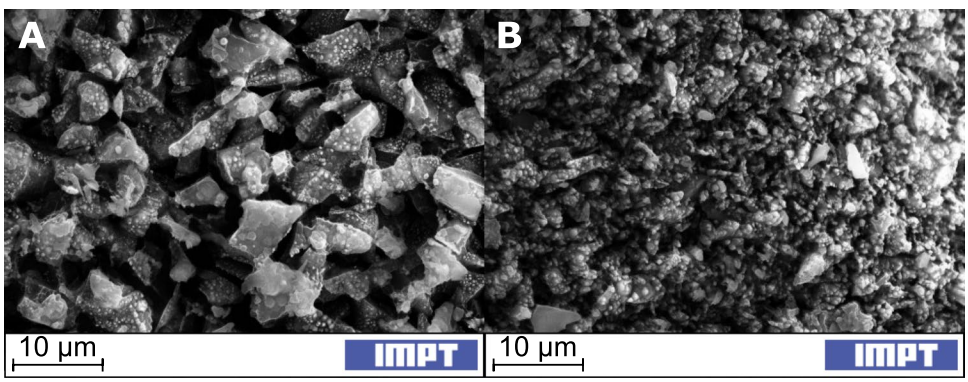

Fig. 3 The figure shows a topography comparison of the different abrasive grains used. In **A**, the surface of a ready-to-use micro-grinding tool with a 4–6 µm grain size is shown; in **B**, grains with a size of 1.6–2.4 µm were used

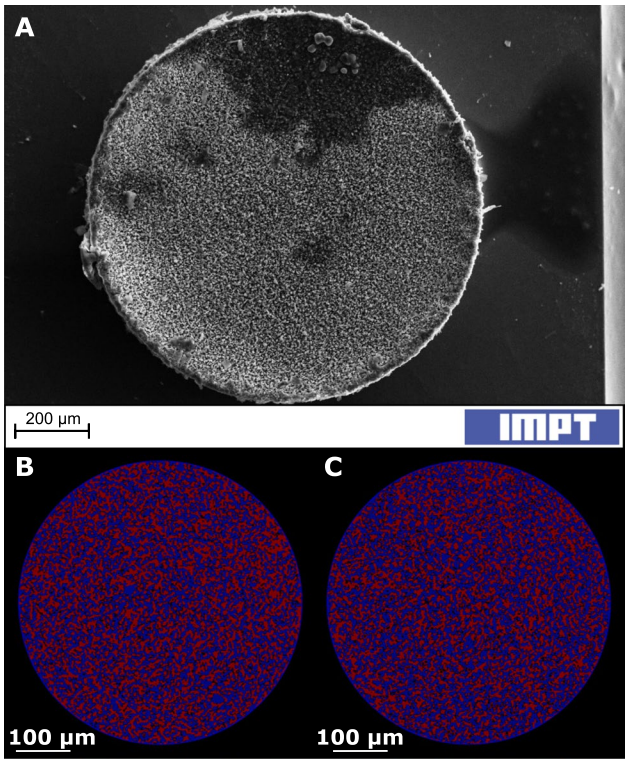

Fig. 4 The figure shows an SEM picture of an exemplary surface (**A**) and the analysis of two sectional views of a micro-grinding tool. The areas digitally coloured in blue reflect the SiC, while the red areas represent the bond matrix. In **B**, a section of the upper half of the abrasive layer, and in **C**, a section of the lower half is shown

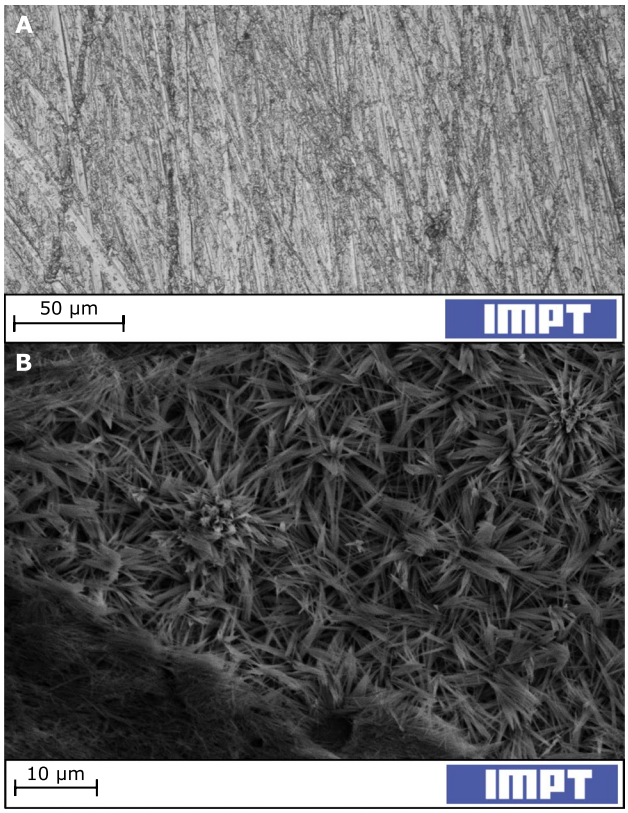

Fig. 5 The figure shows in **A** an image of the copper surface before oxidation, taken with confocal microscopy. In **B**, the figure shows an SEM image of the surface of an anodised copper workpiece. The oxide grows in a needle-like structure with the selected process parameters

rate can be achieved. This should have a positive effect on the grinding process.

3.2 Characterisation of oxidised copper workpieces

To check the result of the anodic oxidation, the oxide layer is examined for its topography and chemical composition. The topographical examination is carried out by means of SEM. Such an image is shown in Fig. 5. From the literature, a surface covered with needle-shaped copper oxide structures could be expected [9]. This was confirmed by the analysis as shown in the figure. The directions in which the individual needles grow are arbitrary. Only the width of the structures seems to be homogeneous. In addition to the already known higher brittleness of copper oxide, the needle-shaped structure of the oxide could lead to better machinability, as less force is needed to break or remove the needles compared to solid material due to their limited thickness. When visually comparing the oxide layers produced outside the machine tool and those produced inside, there is no difference in topography. However, it is important that the process parameters are the same and that the reaction surface and thus the current density are comparable. The remaining materials used in the construction of the electrochemical chamber for the machine tool show no influence on the reaction compared to a reaction in a glass vessel.

In addition to the topography, the chemical composition of the oxide layer is also of interest. Both a non-treated, oxidised sample and an annealed sample were measured by XPS. The results are shown in Fig. 6. The Cu 2p region is shown. The composition of the layer from the different copper oxide forms is of interest. Figure 6A shows the oxide layer directly after anodic oxidation. The first three peaks confirm the presence of Cu^2+ within the oxide layer. The subsequent peaks provide an indication of the form in which the copper is present. Here, a high proportion of $Cu(OH)_2$ is evident. Similarly, the analysis shows a high proportion of Cu_2O and no to barely measurable proportion of CuO. In comparison, Fig. 6B shows the measurement of an annealed sample. Here, a high proportion of Cu_2O can still be detected, but the temperature treatment resulted in a decrease in $Cu(OH)_2$. In return, the proportion of CuO increased significantly. This is also described in the literature [12]. The temperature effect with a temperature above 150 °C converts the $Cu(OH)_2$ into CuO, because a

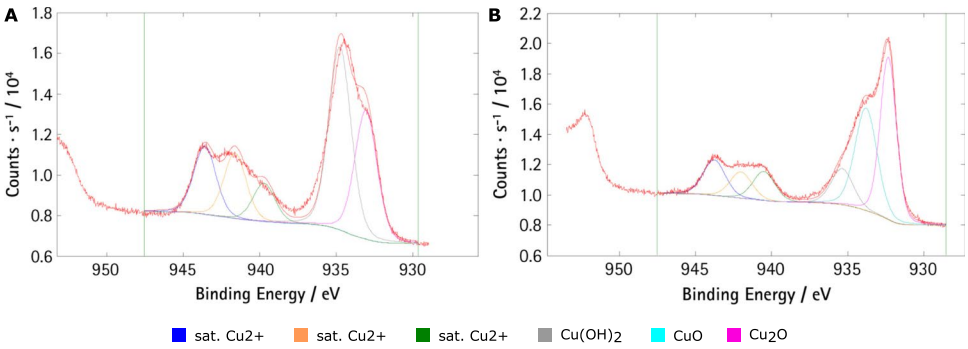

Fig. 6 The figure shows XPS analyses of anodically oxidised copper surfaces. **A** shows the results of the measurement of an untreated sample, **B** of a sample annealed after oxidation. Both show the Cu 2p region

dehydration takes place. Despite the transformation shown by the XPS analysis, no change in topography takes place. An examination by SEM of the annealed copper oxide samples shows an unchanged, needle-like surface structuring. Optically, however, a colour change takes place. Before, the oxide layer shows a light blue colouration, while after annealing, it shows a greenish colour. This is another indication that a chemical transformation took place due to the temperature treatment.

The XPS analysis is only used to understand what kind of oxide layer has been created, but does not by itself indicate whether one or the other chemical composition leads to better machinability. However, it clearly shows that there is a difference in composition. In combination with the following scratch test investigation, a statement can then be made whether additional annealing of the oxide layer could be of significance for the grinding application. Therefore, in the scratch test with an indexable insert, as already described, both pure copper surfaces and the anodically oxidised samples are tested. Due to the known higher brittleness of the copper oxide and the already shown needle-shaped structure of the oxide layer, the indexable insert should need less force to cut through the oxide layers compared to the pure copper.

The results of this are shown in Fig. 7. The curves already show the mean value curves from the five recorded measurements. Below the diagram in Fig. 7B–D, the copper samples after the scratch test are shown in order to compare the scratches on the surface. The circular structure of the scratches results from the rotation of the workpiece while the tool is kept static. All three curves show a strong fluctuation of the required force F_x at the beginning, when the insert enters the surface. After a short time, however, this stabilises for the samples of anodically oxidised copper and annealed copper oxide and settles at a value of between − 0.2 to − 0.3 N. The measurement curve in pure copper, on the other hand, shows a different trend. The fluctuation remains for the whole measurement. The curve is very unsteady with high fluctuations between − 0.1 and − 0.9 N. This alone suggests that the insert does not cut through the pure copper as easily as it does with the oxidised copper samples. This impression is also confirmed when looking at the machined surfaces. The two oxidised copper surfaces (Fig. 7C and D) show a very even scratch with only some defects in a few places, which could come from rattling of the tool. With the pure copper (Fig. 7B), on the other hand, no continuous scratch can be observed. The scratch here is rather interrupted.

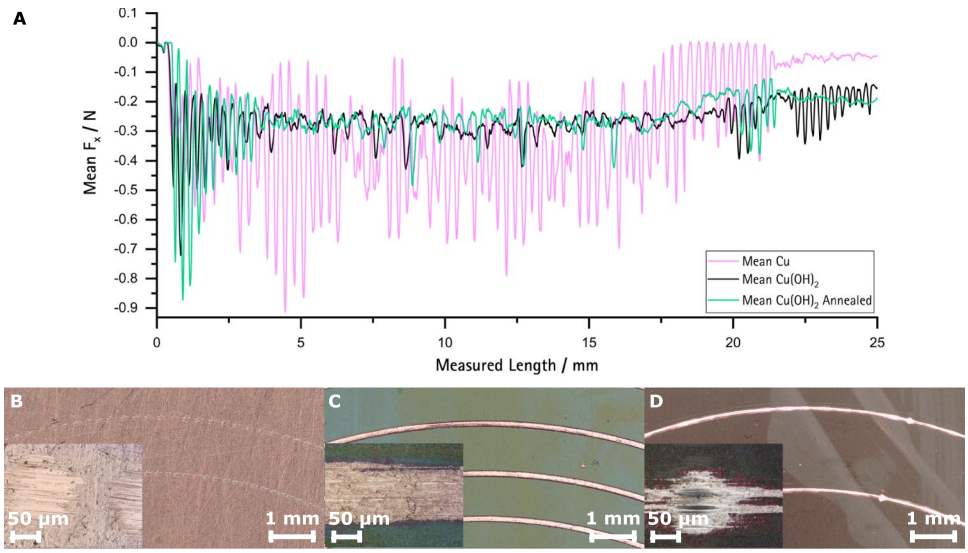

Fig. 7 The figure shows in **A** the forces F_x recorded during the scratch test as a function of time. In **B**, the caused scratches on Cu; in **C**, on $Cu(OH)_2$; and in **D**, on annealed $Cu(OH)_2$ are shown. Furthermore, close-ups of the resulting scratches are added in **B**–**D**

Presumably, the tool rattled continuously over the surface instead of cutting constantly. Due to the force F_z for the penetration of the tool into the surface, which is the same for all samples, it can be concluded that the tool travels more easily and evenly through the oxidised copper than through the pure copper. This is partly due to the higher brittleness of the copper oxide and probably also to the needle-like structure of the oxide layer, as very little force is needed to break the needle structures due to the small diameter compared to the length. However, it can also be observed that there is no significant difference between the anodically oxidised sample and the sample that is annealed. The scratch test shows a similar result for both. It can therefore be assumed that an additional annealing step before machining does not lead to better machinability of the surface. This allows the conclusion that the chemical composition of the oxide layer has a rather minor influence in this case. Therefore, annealing will not be considered in the following grinding test. Also, the duration and the additional need for a heat source would make this process step impractical for the surface modification of the copper workpiece within the machine tool.

The analysis of the anodically oxidised copper surface shown here supports the assumption that the copper oxide produced leads to better machinability and can thus be purposefully incorporated as a surface modification before the grinding process. The surface produced has a composition of needle-shaped structures with a high proportion of $Cu(OH)_2$. However, no dependence of the machinability on the chemical composition could be determined.

3.3 Analysis of the grinding tests

In this publication, the production of micro-grinding tools with smaller abrasive grains was shown, whose usability on copper and copper oxide will be compared in the following with the already described usability of SiC 4–6 µm tools [5, 10]. Therefore, the grinding process is first carried out on a pure copper surface. In the following, the roughness values in Fig. 8, measured by confocal microscopy, are plotted, which could be measured when machining the pure copper workpiece after the grinding process. It is noticeable that the roughness values achieved are in a similar range for both tools used. The course of the curves is also very similar. Already after four grinding iterations, the curve reaches a limit value and hardly drops any further until the measuring point after seven grinding iterations. The SiC 4–6 µm tools achieve a roughness value $R_a = 0.04 \pm 0.02$ µm and $R_z = 2.32 \pm 0.59$ µm. The tools with the 1.6–2.4 µm grains achieve similar values. After seven grinding iterations, an R_a value of 0.09 ± 0.02 µm and an R_z value of 1.94 ± 0.73 µm can be measured. Thus, the exclusive use of the 1.6–2.4 µm tools shows no advantage over the use of the tools with larger grains. The only advantage could be the lower tool

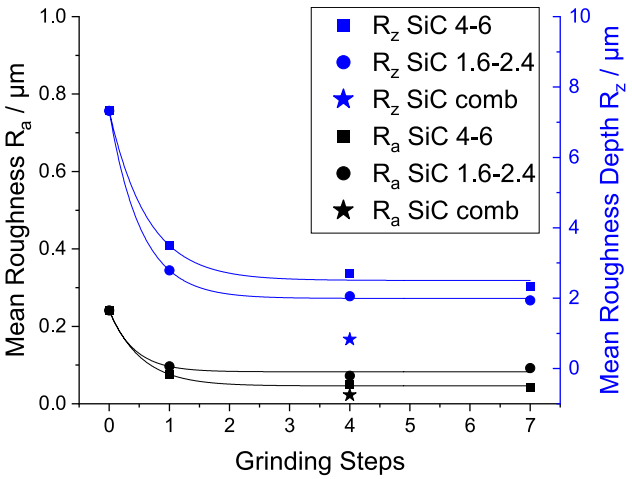

Fig. 8 The figure shows the progression of the roughness values of the copper surface after a different number of grinding iterations. Blue represents the values for R_z, black the values for R_a. The values for the roughness values achieved with the SiC 4–6 µm tools are taken for comparison from an earlier work [5]

wear. Here, an average wear of the grinding layer of 5.07 ± 3.38 µm was measured with the SiC 4–6 µm tools in the first two grinding iterations and 0.92 ± 2.01 µm in iterations 3–7. The 1.6–2.4 µm tools initially showed a wear of 2.58 ± 2.36 µm and 0.68 ± 1.91 µm in the following five grinding iterations. Thus, both the initial wear and the subsequent wear are lower for the tools with the smaller grain size. This is probably proportional to the grain size. The initiative wear is greater for both tool types, as the etching process leaves the upper grains significantly more exposed and therefore more easily broken out. When a grain layer wears and breaks out, the tool wear is therefore significantly greater with larger grains than with smaller grains. However, it is also important to note the high standard deviation, which could let the described effect seem to be greater than it is.

Since the use of SiC 1.6–2.4 µm tools did not lead to any improvement of the surface roughness, a grinding process with combined tool use is tested. For this purpose, the first two grinding steps are carried out with the large-grained tool and then two fine grinding steps with the small-grained tool. The roughness values achieved are also shown in Fig. 8. Both roughness values here are below those that could be produced by using one tool type only. After the four grinding iterations, the value for R_a is 0.02 ± 0.01 µm and for R_z 0.83 ± 0.21 µm. Especially for R_z, a significant reduction of the value can be seen after a total of four grinding iterations instead of the previous seven. This can be explained analogously to the usual procedure in grinding processes. The larger grains result in a higher removal of material, which removes most of the roughness, but may also introduce new grinding scratches due to the grain size. The subsequent use of finer grain leads to the repair of the defects introduced

by the larger grain and thus to a further smoothing of the surface.

Since it has already been shown that oxidation of the surface leads to a better surface roughness during the grinding process [10] and the combined use of both tool types on pure copper also results in an improvement of the grinding process, both processes are now to be combined within the machine tool. For this purpose, the samples oxidised in the machine are machined with the combined grinding process, and the roughness values are measured. The machined surface shows roughness values of $R_a = 0.03 \pm 0.01$ µm and $R_z = 0.69 \pm 0.20$ µm. Whereas no improvement is visible in R_a, the R_z value is reduced by a further 17% from the value on a pure copper surface before due to the combination of oxidation and grinding process.

4 Conclusion

Previous work has already demonstrated the use of SiC micro-grinding tools on copper and copper oxide. Using 4–6 µm SiC grains as abrasives, it has already been possible to achieve a surface roughness of $R_a = 0.04 \pm 0.02$ µm and $R_z = 2.32 \pm 0.59$ µm on copper [5, 10]. On copper oxide, an improvement of the surface quality to $R_a = 0.04 \pm 0.02$ µm and $R_z = 1.10 \pm 0.35$ µm could be achieved [10]. In this work, the production of micro-grinding tools with grain sizes 4–6 µm and, in addition, 1.6–2.4 µm was analysed. Computer tomographic analysis showed that after manufacturing, a homogeneous grain distribution exists within the abrasive layer. Comparing the grinding results, the use of SiC 1.6–2.4 µm tools alone did not improve the roughness values. By using a combination of both tool types on pure copper, the surface quality could be further improved ($R_a = 0.02 \pm 0.01$ µm, $R_z = 0.83 \pm 0.21$ µm). Only four grinding iterations, two per tool type, compared to seven for the SiC 4–6 µm tools, were needed with this grinding strategy. Moreover, the surface modification of the copper was researched. Here, anodic oxidation in NaOH using XPS measurement revealed a high proportion of $Cu(OH)_2$, which can be converted into CuO by annealing at 200 °C. In a scratch test, both oxide layers showed better machinability compared to pure copper, whereby no dependence on the chemical composition could be detected. To transfer the process into the machine tool, an electrochemical cell was presented. With this setup, the grinding of the copper surface can be electrochemically assisted. This resulted again in improved roughness values. While $R_a = 0.03 \pm 0.01$ µm remained similar to before, R_z was reduced by another 17% to $R_z = 0.69 \pm 0.20$ µm. Thus, an electrochemically assisted grinding process with batch-manufactured flexible micro-grinding tools could be successfully integrated in the machine tool. It was demonstrated that the developed grinding procedure leads to the best surface finishes achieved with these micro-grinding tools so far.

In the future, further development is possible. A more targeted oxidation of only local structures would reduce the chemical exposure of the rest of the workpiece and, due to the smaller reaction area, could increase the current density and thus the reaction rate. Moreover, an extension to other materials, such as silicon, would greatly expand the functional range of the tools.

Author contribution All authors contributed to the study conception and design. The experiments and their analysis were performed by Lukas Steinhoff. The first draft of the manuscript was written by Lukas Steinhoff, and all authors commented on previous versions of the manuscript. All authors read and approved the final manuscript.

Funding Open Access funding enabled and organized by Projekt DEAL. The work was funded by the German Research Foundation (DFG, Deutsche Forschungsgemeinschaft)-Project "Batchprocessed flexible micro-grinding tools for end machining of metallic surfaces" (WU 558/26–1).

Declarations

Competing interests The author declares no competing interests.

References

1. Harvey JE, Lewotsky KL, Kotha A (1995) Effects of surface scatter on the optical performance of x-ray synchroton beam-line mirrors. Appl Opt 34:3024–3032. https://doi.org/10.1364/AO.34.003024
2. Brinksmeier E, Preuss W (2012) Micro-machining. Phil Trans R Soc A 370:3973–3992. https://doi.org/10.1098/rsta.2011.0056
3. Kuyucak S, Sahoo M (1996) A review of the machinability of copper-base alloys. Can Metall Q 35:1–15. https://doi.org/10.1179/cmq.1996.35.1.1
4. Heintze SD, Forjanic M, Rousson V (2006) Surface roughness and gloss of dental materials as a function of force and polishing time in vitro. Dent Mater 22:146–165. https://doi.org/10.1016/j.dental.2005.04.013
5. Steinhoff L, Dencker F, Wurz MC (2022) Euspen's 22nd International Conference & Exhibition, Geneva, CH
6. Gäbler J, Pleger S (2010) Precision and micro CVD diamond-coated grinding tools. Int J Mach Tools Manuf 50:420–424. https://doi.org/10.1016/j.ijmachtools.2009.10.008

7. Kirsch B, Bohley M, Arrabiyeh PA, Aurich JC (2017) Application of ultra-small micro grinding and micro milling tools: possibilities and limitations. Micromachines 8:261–279. https://doi.org/10.3390/mi8090261
8. Park J, Kim D, Kim H, Park WI, Lee J, Chung W (2022) Superhydrophobic electrodeposited copper surface for robust condensation heat transfer. ACS Omega 7:19021–19029. https://doi.org/10.1021/acsomega.2c02522
9. Wu X, Bai H, Zhang J, Chen F, Shi G (2005) Copper hydroxide nanoneedle and nanotube arrays fabricated by anodization of copper. J Phys Chem 109:22836–22842. https://doi.org/10.1021/jp054350p
10. Steinhoff L, Dencker F, Wurz MC (2023) Application of batch manufactured flexible micro-grinding tools on copper and oxidized copper surfaces. Tribol Schmier.tech 70(1):5–10. https://doi.org/10.24053/TuS-2023-0002
11. International Organization for Standardization (1997) ISO 4287:1997–04: Geometrical product specifications (GPS) - surface texture: profile method - terms, definitions and surface texture parameters. Berlin: Beuth
12. Wu X, Shi G (2006) Production and characterization of stable superhydrophobic surfaces based on copper hydroxide nanoneedles mimicking the legs of water striders. J Phys Chem 110:11247–11252. https://doi.org/10.1021/jp056969x